Transient Moisture and Heat Transfer in Multi-Layer Non-Isothermal Walls—Comparison of Predicted and Measured Results

D.M. Burch **W.C. Thomas** **L.R. Mathena** **B.A. Licitra** **D.B. Ward**

ABSTRACT

A distributed-capacity, finite-difference model is presented for predicting the transient heat and moisture diffusion through a multilayer plane wall. The model is one-dimensional and uses a single potential (i.e., water vapor pressure) to predict the moisture transfer rate.

This model was used with independently measured moisture properties to predict the results of a simple experiment. Two plane walls, measuring 2 ft by 2 ft by 4.5-in. thick (0.61 by 0.61 by 0.11 m) were exposed to a step decrease in temperature and humidity at their exterior surfaces. The walls were comprised of gypsum board with interior latex paint, cavity insulation, and white pine with exterior oil-base paint. One of the walls was insulated with glass-fiber insulation, the other with cellulose insulation. Moisture was permitted to accumulate within the walls during a 34-day period. The model predicted with good agreement the accumulation of moisture in the wood.

Laboratory methods to measure independently the moisture properties of the materials are also described. The effect of moisture accumulation on the overall thermal resistance of the two walls was investigated.

INTRODUCTION

During the winter season in cold regions, the specific humidity, or moisture content, of the air within buildings is considerably higher than that of the outdoor air. As a result, moisture permeates into walls and becomes absorbed within the wall materials, particularly the outer layers. A significant buildup of moisture within these materials may have an adverse effect on their thermal insulating, structural strength, and durability properties.

Mathematical models (Kohonen 1984; Andersson 1985) for predicting time-dependent moisture transfer within building components are just now evolving. A reliable and validated mathematical model is not yet available for predicting the time-dependent moisture accumulation within multilayer walls and roof assemblies found in practice. Consequently, experimentation and previously related experience are about the only proven approaches available to aid building designers in avoiding moisture problems while minimizing heat loss. Experimentation on individual components is, of course, costly and time-consuming, and specific results cannot be readily extended to different geometries and exposure conditions.

D. M. Burch is a mechanical engineer, National Institute of Standards and Technology, Gaithersburg, Maryland; W. C. Thomas is a Professor of Mechanical Engineering, Virginia Polytechnic Institute and State University, Blacksburg, Virginia; L. R. Mathena is an Engineering Trainee; B. A. Licitra is a Computer Specialist; and D. B. Ward is an Engineering Technician at the National Institute of Standards and Technology, Gaithersburg, MD.

A motivation for the present research is to provide a basis to extend individual experiments to different constructions and different indoor and outdoor conditions. Mathematical models, capable of performance simulations, will hopefully serve as a means of communication between various building scientists. The long-term objective is to develop guidelines for controlling moisture in new and existing building walls.

MATHEMATICAL MODEL

While diffusion and convection (i.e., infiltration) through porous materials and penetrations in the building envelope are both recognized as important modes of moisture transfer in typical buildings, the current analysis is limited to transfer by molecular diffusion as a necessary step in the evolution of a more general treatment.

A composite plane wall with N permeable slabs in series, as shown in Figure 1, is analyzed. Initially, each slab has an arbitrary moisture content distribution. The exterior surfaces are suddenly exposed to ambient environments with time-varying temperature and water vapor pressure. The variation of moisture content and temperature in the slabs as a function of time is analyzed.

The following assumptions are used in the analysis:

- Moisture transfer by diffusion in the porous matrix layers is proportional to the vapor partial pressure gradient and permeability. Moisture concentration is below the fiber saturation point (i.e., no free liquid or ice is present in any of the materials).
- Heat and moisture transfer are one-dimensional.
- The effects of moisture content and temperature variations on the permeance of materials are neglected. Either a wet- or dry-cup value is used.
- The sorption isotherm is based on the average of adsorption and desorption data (i.e., hysteresis and temperature effects are neglected).
- Vapor adsorption at a surface releases the latent heat of vaporization and vice versa. Enthalpy transfer within porous layers is neglected.

Some additional assumptions are introduced later.

Moisture Transfer

Differential Equation. Within each layer n of Figure 1, moisture transfer is governed by the following conservation of mass equation:

$$\frac{\partial}{\partial x}\left(\mu_n \frac{\partial p}{\partial x}\right) = \frac{\partial \theta}{\partial t} \tag{1}$$

Introducing the sorption isotherm relation in terms of $\phi = p/p_g$

$$\gamma_n = \frac{\theta_n}{\rho_n} = f_n(\phi, T) \simeq f_n(\phi) \tag{2}$$

and the specific moisture capacity defined as

$$G_n = \left(\frac{d\gamma}{d\phi}\right)_n \tag{3}$$

Equation 1 becomes:

$$\frac{\partial}{\partial x}\left(\mu_n \frac{\partial}{\partial x}\left(\phi p_g\right)\right) = \rho_n G_n \frac{\partial \phi}{\partial t} \tag{4}$$

Temperature has a strong effect on the saturature pressure (p_g).

Initial and Boundary Conditions. Within each layer, the initial moisture content is arbitrary, or:

$$\gamma_i(x,o) = g_i(x) \tag{5}$$

At the inside wall surface (see Figure 1), the moisture transfer by convection to the first layer is equal to the moisture transfer by diffusion into the material, or:

$$M_{er}(p_r - p) = -\mu_1 \frac{\partial p}{\partial x} \quad \text{at } x = 0 \tag{6}$$

where M_{er} denotes "an effective permeance" at the surface, equivalent to a moisture transfer conductance. At the exterior wall surface, a similar relation applies:

$$M_{ec}(p - p_c) = -\mu_N \frac{\partial p}{\partial x} \quad \text{at } x = L \tag{7}$$

In Equations 6 and 7, the effect of a thin paint or plastic film is taken into account as a surface conductance (M_p) in series with the surface conductance (M_f) associated with the convective mass transfer coefficient rather than being treated as an additional layer. The effective surface conductance (M_e) is defined by:

$$\frac{1}{M_e} = \frac{1}{M_f} + \frac{1}{M_p} \tag{8}$$

At each of the interfaces, the water vapor pressure is continuous across the boundary between the layers.

Heat Transfer

Differential Equation. Within each layer n, heat transfer is governed by the following conservation of energy equation:

$$\frac{\partial}{\partial x}\left[k_n \frac{\partial T}{\partial x}\right] = \rho_n (C_{dn} + \gamma C_{fn}) \frac{\partial T}{\partial t} \tag{9}$$

Enthalpy transport by water vapor in wall systems is very small and therefore was neglected in the present analysis. The thermal conductivity (k_n) is an effective value that includes the effect of heat conduction through bound water in the material. The term ($C_{dn} + \gamma C_{fn}$) includes the effect of energy storage in bound water.

Initial and Boundary Conditions. Within each layer, the initial temperature is arbitrary, or:

$$T_i(x,o) = r_i(x) \tag{10}$$

At the inside wall surface, convection from the indoor air equals heat conduction into the first layer plus the heat released by adsorbed moisture, or:

$$h_r(T_r - T) = -k_1 \frac{\partial T}{\partial x} + \dot{n}''_r \cdot \lambda \quad \text{at } x = 0 \tag{11}$$

At the outside surface, a similar relation applies, or:

$$h_c(T - T_c) = -k_N \frac{\partial T}{\partial x} + \dot{n}''_c \cdot \lambda \quad \text{at } x = L \tag{12}$$

Solution Procedure

Equations 1 through 12 were recast into finite-difference equations using a uniform nodal spacing within each layer. An implicit solution technique with coupling between the two

conservation equations was used to solve the equations. A FORTRAN 77 computer program with an efficient tridiagonal matrix solution algorithm (Carnahan et al. 1964) was prepared. The calculations proceed by first solving for the temperature distribution and then the relative humidity or vapor pressure distribution, which specifies the moisture content distribution. By choosing a sufficiently small time step, the need for iteration to account for moisture concentration- and temperature-dependent properties in the implicit solution method was eliminated. The procedures for measuring the permeability and sorption isotherm for the various materials are presented in the next section.

The accuracy of the numerical solution depends on both the nodal spacing and the time step. Progressive smaller nodal spacing and time steps were used to ensure convergence of the finite-difference solution.

EXPERIMENTAL MEASUREMENTS

Wall Moisture Accumulation Experiment

Description of Experimental Setup. A conditioning chamber was installed inside an environmental room, as shown in Figure 2. Two wall specimens, each 2 ft by 2 ft (0.61 by 0.61 m), were installed in a polystyrene support frame of the conditioning chamber. The inside surfaces of the wall specimens were exposed to the ambient conditions of the environmental room, while the outside surfaces were exposed to the ambient conditions within the conditioning chamber.

The wall specimens consisted of 0.52 in. (13 mm) gypsum board, 3.5 in. (89 mm) cavity insulation, and 0.51 in. (13 mm) white pine. The interior surface of the gypsum board was painted with a latex paint system (i.e., two coats of latex primer and two coats of latex finish). The exterior surface of the white pine was painted with an oil-base paint system (i.e., two coats of oil-base primer and two coats of alkyd finish). The upper wall specimen was insulated with loose-fill cellulose insulation with a density of 4.96 lb/ft^3 (79.5 kg/m^3), while the lower was insulated with glass-fiber batt insulation with a density of 0.716 lb/ft^3 (11.5 kg/m^3).

The conditioning chamber consisted of an upright domestic freezer with a fan and electric heater installed inside at the bottom, as shown in Figure 2. When the conditioning chamber was operated, the temperature control supplied with the freezer was set at its lowest setting so that the freezer's refrigeration system operated continuously. The desired ambient condition was achieved by regulating the heater output using a proportional controller. Trays of desiccant were placed on the shelves of the freezer to maintain a low relative humidity, thereby preventing excessive frost accumulation on the refrigeration evaporator coil.

Instrumentation. Measurements to determine temperature distributions, air humidity, and moisture content of the white pine were made during the experiments on the wall specimens. Sensor locations are shown in Figure 3.

The ambient air temperature 3 in. (7.6 cm) from the inside and outside surfaces of each wall specimen was measured with a 24-gauge, copper-constantan thermocouple. The relative humidity within the environmental room was measured with an electric-resistance sensor located about 3 in. (7.6 cm) from the inside surface and at the mid-height of the freezer. The dewpoint temperature within the conditioning chamber was measured with a chilled-mirror dewpoint hygrometer.

Five moisture content sensors, based on the electrical resistance principle, were installed to periodically measure the moisture content at the inside wood surfaces of both wall specimens at the locations shown in Figure 3. Another moisture content sensor was installed to measure the moisture content at the center of the outside wood surface. Each sensor consisted of two parallel conductive epoxy strips, 7/8-in. (22 mm) long, 1/8-in. (3.2 mm wide), bonded to the wood surface. The epoxy strips were placed 0.5-in. (13 mm) apart across the grain of the wood. Lead wires were attached to the ends of the epoxy strips and connected to an electrical-resistance meter, calibrated to read out moisture content directly. The sensors and the resistance meter were calibrated for white pine at the temperatures attained by the wood during the experiment.

Thermocouples constructed from 24-gauge copper-constantan wire were attached to the wood surface at each of the locations where the moisture content sensors were installed.

The temperature difference across the gypsum board was measured with a thermopile to determine the heat flux at the inside surface. The individual thermocouple junctions were spread out in a vertical rake (see Figure 3) so as to be non-intrusive to moisture transfer. The heat flux was taken as the sensed temperature difference divided by the thermal resistance of the gypsum board. Here it was assumed that the thermal resistance of the gypsum board was constant. The effect of moisture content on its thermal resistance was neglected because the moisture content of gypsum board, which is weakly hygroscopic, does not vary significantly with relative humidity.

A data acquisition system recorded the above measurements (except for the moisture content sensors) at hourly intervals. The moisture content sensors were recorded manually once a day except on weekends.

Boundary Conditions. The pre-conditioning and conditioning ambient conditions generated in the conditioning chamber are shown in Figure 4.

The inside and outside surfaces of the two wall specimens were initially pre-conditioned to an ambient environment at 75° ± 0.6°F (24° ± 0.3°C) and 51% ± 2.1% RH for a 67-day period, thereby permitting the wall components to equilibrate at this condition.

At the start of the conditioning period, the temperature and relative humidity within the conditioning chamber were decreased within a one-hour period to 34°F (1°C) and 7% RH, respectively. The temperature and relative humidity within the environmental room were maintained at the initial condition. From Figure 4B, it is seen that the relative humidity in the conditioning chamber was initially decreased markedly by the desiccant in the trays. As the desiccant absorbed moisture and its drying capacity diminished, the relative humidity rose until the dewpoint temperature of the air became approximately equal to the surface temperature of the refrigeration evaporator coil.

At the conclusion of the 34-day conditioning period, 1-in. (25 mm) diameter samples of the white pine were cored 2-in. (51 mm) above each location where moisture content sensors were installed. The cores were cut out with a slow-speed circular hole saw. The heating effect was small since no temperature change could be detected based on touch. Each of the cores was sliced into two half-thickness disks, and the moisture content of each half was determined gravimetrically using desiccant drying.

After the 34-day conditioning period, the moisture contents indicated by the moisture content sensors were significantly higher than cored values and had to be disregarded. It was found that the electrical fields from the refrigeration system and blower of the conditioning chamber interfered with the moisture content sensors. However, prior to the 34-day conditioning period, when the refrigeration system and blower were off, the moisture content sensors gave correct readings.

Moisture Sorption Isotherm Measurements

White pine and gypsum board specimens, approximately 0.7 $in.^3$ (1.1 x 10^{-5} m^3), were placed on a support and sealed in pint-size jars, as shown in Figure 5. Insulation specimens were held in small plastic containers having a known empty weight. These containers were approximately 1 $in.^3$ (1.6 x 10^{-5} m^3) in volume and made of a nonhygroscopic perforated plastic. Calcium-chloride desiccant and the eight saturated salt-in-water solutions listed in Table 1 were used for a relative humidity range within the jars up to 96%. The jars were maintained at a constant laboratory temperature of 76° ± 1°F (24° ± 0.5°C). Each specimen was conditioned in a separate jar and periodically weighed until its weight indicated that equilibrium with the relative humidity inside the jar had been established. Equilibrium was deemed to exist when no further change in specimen weight occurred during a four-week period. After reaching equilibrium, the specimens were removed from the jars and quickly weighed on a precision balance having a resolution of 2.2 X 10^{-7} lb (1 X 10^{-4} gram).

The dry weights of the specimens were determined in jars containing calcium-chloride ($CaCl_2$) desiccant. The equilibrium RH above this desiccant was 1.4% (Baxter and Starkweather 1916). Desiccant drying, as opposed to oven drying, was used to remove moisture, thereby preventing the removal of other volatiles or causing chemical changes in the specimens. The moisture content was determined by taking the difference between the moist and dry weights

and dividing by the dry weight.

A typical measured equilibrium moisture content vs. relative humidity is shown in Figure 6 for white pine. For the desorption isotherm (dotted upper curve), the specimens were initially conditioned to their fiber-saturation state by placing them in a sealed container above liquid water. The specimens were subsequently placed in jars with the saturated salt solutions. For the adsorption isotherm (dotted lower curve), the wood specimens were initially conditioned to a dry state with $CaCl_2$, and then with the saturated salt solutions. The solid line in Figure 6 depicts a fit to the mean of the adsorption and desorption data using an equation of the form:

$$\gamma(\phi) = \frac{a_1\phi}{\left[1+a_2\phi\right]\left[1-a_3\phi\right]} \tag{13}$$

where a_1, a_2, and a_3 are empirical constants determined by a regression analysis. This functional form is based on the activation energy theory for wood (Simpson 1971). Equation 13 was found to correlate data extremely well for all the materials. This model has the advantages of covering the entire humidity range with a small root-mean-square residual error and can also be solved explicitly for ϕ as a function of γ.

The empirical constants for all the materials tested are summarized in Table 2. When the empirical constants are substituted in Equation 13, the equilibrium moisture contents for gypsum board and glass fiber insulation are found to be considerably less than those of wood or cellulose.

Transport Property Measurements

Steady-state water vapor transmission measurements for the materials were carried out in accordance with the procedures outlined in ASTM E 96-80 (ASTM 1988), as indicated below. For these measurements, specimens of the materials were installed in permeance cups, as shown in Figure 7. A dry-cup measurement was judged to represent best moisture transport within the layers of the wall toward the inside surface (i.e., gypsum board, cavity insulation, and latex paint), and a wet-cup measurement would best represent moisture transport within the layers nearest the outside surface (i.e., white pine and oil paint).

For the wet-cup measurements, a potassium nitrate saturated salt solution, rather than distilled water (as specified in ASTM E 96-80 [ASTM 1988]), was used inside the cup. The equilibrium RH above this saturated salt solution is 93.6% at 77°F (25°C). The use of a wet-cup relative humidity slightly less than saturated was believed to reduce the possibility of condensate droplet formation at the lower surface of the specimen. For the dry-cup measurements, calcium-chloride desiccant was used inside the cup. For all the measurements, the permeance cups were placed in an environmental room maintained at steady 53° ± 2.1% RH and 75° ± 0.6°F (24° ± 0.3°C) dry-bulb temperature.

After the cups were set up as described, they either gained or lost weight as a result of water transfer through the specimen. The mass transfer flux ($\dot{n}''$) for each of the cups was determined by periodically weighing it and dividing by the exposed surface area of the specimen (0.190 ft^2, 0.0177 m^2). For each of the cup tests, the total moisture-transfer resistance (R_t) of the specimen was calculated using:

$$R_t = \frac{p_g\left[\phi_r - \phi_c\right]}{\dot{n}''} \tag{14}$$

Air Film Resistance. A special series of water vapor transfer measurements were conducted to determine the resistance to moisture transfer resulting from the convective mass transfer coefficients at the upper surface of the specimen and inside the cup.

For these measurements, one, two, three, and four layers of 0.11-in. (2.8-mm)-thick cork board were installed in permeance cups with calcium-chloride desiccant. The measured total resistance for these cup tests was plotted as a function of thickness (number of layers), as shown in Figure 8. Since the plot is clearly linear, the total film resistance is constant (i.e., independent of the moisture transfer rate and moisture distribution in the cork). The

ordinate intercept is, therefore, the overall film resistance (R_f = 0.020 h-ft^2-inHg/grain, 3.48 X 10^8 s-m^2-Pa/kg) for moisture transfer. This resistance, which is not normally considered in cup-test procedures, is significant – about the same as that of 0.5-in.-thick (13-mm) gypsum board.

Solid Materials. The permeability of gypsum board and white pine were determined from:

$$\mu = \frac{\ell}{R_t - R_f} \tag{15}$$

where ℓ is the thickness of the material.

Surface Coatings. After the dry-cup measurement of the gypsum board specimen was completed, its upper surface was coated with a latex paint system (i.e., two coats of latex primer and two coats of latex finish). The latex paint system was permitted to dry for several days. The cup was subsequently periodically weighed, and the total moisture transfer resistance was determined using Equation 14. The permeance (M_p) of the latex paint system was determined by:

$$M_p = \frac{1}{R_t - R_s} \tag{16}$$

Here R_s is the substrate resistance for the gypsum board.

After the wet-cup measurement of the white pine was carried out, its upper surface was coated with an oil-base paint system (i.e., two coats of oil-base primer and two alkyd finish coats). The permeance of the oil-base paint system was determined from two wet-cup measurements in a similar fashion as that used for the latex paint system.

Thermal Insulation Materials. Two dry cups were prepared with a single layer of cork installed in each. The purpose of the cork was to support the insulation. A 3.5-in. (89 mm)-high vapor-impermeable sleeve was sealed above each of the cups over the measuring area. Glass fiber insulation with a density of 0.716 lb/ft^3 (11.4 kg/m^3) was installed in the sleeve of one cup, and cellulose with a density of 4.11 lb/ft^3 (65.8 kg/m^3) in the other. The moisture-transfer resistance for the cork-insulation assemblies (R_t) and for each of the cork layers (R_s) was determined as described above. The resistance for each of the insulations was determined by subtracting the resistance of the cork substrate from that for the cork-insulation assembly. The permeability (μ_i) for each of the thermal insulations was determined by:

$$\mu_i = \frac{\ell}{R_t - R_s} \tag{17}$$

where R_s is the substrate resistance for the cork layer.

The moisture transfer properties determined from the above measurements are summarized in Table 3.

PREDICTED AND MEASURED RESULTS

In this section, moisture contents are expressed in percent of the dry weight.

Lateral Moisture Content Distribution

The cored samples of the white pine taken at the end of the 34-day conditioning period revealed a substantial lateral distribution of moisture content. This finding was unexpected because of the precautions taken to design an experiment with one-dimensional moisture transfer. The cored sample data are analyzed below.

When the conditioning chamber was opened up to obtain the core samples, the wood panel next to the glass fiber insulation was observed to have warped, resulting in a crack between the panel and the edge framing. This crack was approximately 1/8-in. (3 mm) wide by 4 in.

(100 mm) long and on the side diagonally opposite from the location of the moisture and temperature sensors.

It was not possible to determine from the data trends when the crack developed. This small aperture was judged to cause only a local effect instead of affecting the overall lateral moisture distribution. This assumption is based on the following observed trends and reasoning. A steady-state diffusion calculation to estimate the moisture transfer through the stagnant air layer of the crack showed that it was small compared to the total transfer through the wood panel. Moreover, the analysis of the trends and distributions indicated by the thermocouples, moisture sensors, and core samples gave no evidence that the crack affected the overall results. The unexpected warpage is called to the attention of the reader as an experimental anomaly and is not considered further in analyzing the data and results for this wall specimen.

In Figure 9, the moisture content at the inside wood surface is plotted as a function of surface temperature for the glass-fiber-insulated wall specimen (upper curve) and cellulose insulated wall specimen (lower curve). The numbers above the symbols "o" and "□" denote the sensor locations given in Figure 3. Heat conduction through the sides of the support frame apparently caused the sides of the wall specimen to be warmer than the center. Note that the surface moisture content correlates approximately linearly with the measured surface temperature. These results indicate that the presence of a 4°F (2°C) lateral temperature difference along the wood surface caused a variation in surface moisture content (dry basis) ranging from 12% to 22% in the glass fiber wall specimen and 10% to 19% in the cellulose wall specimen.

While the measured lateral temperature gradient produces a small departure from one-dimensional heat flow, the resulting lateral vapor pressure gradient can apparently be much more significant. Since the lateral moisture-transfer resistance offered by either of the two insulation materials was relatively small compared to the transverse resistance for the whole wall specimen, a strong lateral moisture transfer took place in the highly porous cavity insulation.

Comparison of Measured vs. Predicted Moisture Contents

The finite-difference model was used to predict the moisture content within both wall specimens. In the finite-difference analysis, the gypsum board, cavity insulation, and wood were subdivided into 3, 10, and 5 nodes, respectively. A one-hour time step was used in the analysis. Since the model was one-dimensional, it did not account for lateral moisture transfer described in the previous section. At any position within the wall, the model predicted a moisture content that would represent an average value for a lateral section of the wall. Thermal and moisture properties used in model are summarized in Tables 2 through 4.

The predicted wood moisture content is plotted as a function of time in Figure 10a for the glass fiber wall specimen and in Figure 10b for the cellulose wall specimen. In each plot, the upper curve is for the inside wood surface and the lower curve is for the outside wood surface. The predicted results are compared to the measured moisture contents determined by the moisture content sensors at the beginning and the core measurements at the end of the 34-day conditioning period. The cored values shown are area-averaged values at the inside and outside wood surfaces.

For both wall specimens, the model predicted with good agreement the accumulation of moisture in the wood during the 34-day conditioning period. Here the term "moisture accumulation" denotes the difference between the final and initial moisture content. At the inside surface of the glass fiber wall specimen, the measured accumulation of moisture was 10.6% compared to a predicted value of 9.3%. At the inside surface of the cellulose wall specimen, the measured moisture accumulation was 7.8% compared to a predicted value of 7.2%. For both wall specimens, a larger difference between measured and predicted values was observed at the outside surface of the wood.

The above comparisons suggest that a considerably more comprehensive model may be needed to predict more accurately the results of this relatively simple experiment. While a two-dimensional model is indicated, such an extension may well require even more property data since these materials are likely to be nonisotropic. Moreover, moisture transport properties were assumed constant while information in the literature indicates that moisture transport properties depend significantly on moisture content and perhaps temperature.

It is interesting to observe that the model predicted that if the experiment were continued an additional 30 days, then wood moisture contents would rise an additional 5% in the glass fiber wall specimen and 4% in the cellulose wall specimen. This would cause moisture contents above 20% to occur. Moisture contents above 20% and approaching the fiber saturation point (27%) previously have been identified as being capable of causing deleterious effects in wood-frame cavity walls (Anderson 1972).

The above results indicate that when a separate vapor retarder is omitted, as in the test sections, diffusion transfer in a well-sealed wall can lead to potentially damaging moisture contents. The boundary conditions of the experiment were not unrepresentative of conditions in residences. Ambient conditions maintained inside the environmental room (i.e., 75°F (24°C) and 51% RH) are representative of a moderately humidified house. The temperature maintained in the conditioning chamber (i.e., 34°F [1.1°C]) is equivalent to a December through February average temperature for many parts of the central U.S.

Both the predicted and measured results shown in Figure 10 and the measured results shown in Figure 9 indicate that the wood moisture contents in the cellulose wall specimen are a couple of percent less than those in the glass fiber wall specimen. A likely reason is that a portion of the moisture that diffuses toward the wood surface in the cellulose wall specimen is stored in the cellulose insulation instead of being stored in the wood. In the glass fiber wall specimen, on the other hand, little moisture is stored in the insulation, and almost all of the diffused moisture is stored in the wood. Moisture accumulations within the two insulations are considered below.

Predicted moisture content distributions at various elapsed times are plotted in Figure 11. Note that the finite-difference model predicts only a very small accumulation of moisture in the glass fiber insulation. On the other hand, the model predicts significant accumulation of moisture in the cellulose insulation.

It should also be noted that an earlier mathematical model by Thomas and Burch (1989) using moisture concentration as the transfer potential failed to predict the observed moisture accumulation in the present nonisothermal experiments. While the earlier model gave results in excellent agreement with data for single layers under isothermal conditions, it predicted a continuous decrease in moisture content in the wood panels for the present experimental conditions rather than the observed accumulation.

Effect of Moisture on Wall Thermal Resistance

The results presented above show that moisture was continuing to accumulate within the wall when the experiment was terminated. The finite-difference model indicated, however, that this rate of accumulation was 6.6×10^{-5} lb/ft^2–h (9.0×10^{-8} kg/m^2–s). The energy storage corresponding to the latent heat release from this adsorbed moisture was calculated and found to be less than 0.5% of the heat flux measured at the inside surface. As a result, steady-state conditions were assumed to exist when analyzing the apparent thermal resistance of the walls.

The daily average thermal resistance of each multilayer wall specimen was determined by dividing the sum of 24 hourly heat fluxes by the sum of 24 hourly overall temperature differences. The heat flux was determined by the thermopile heat-flux transducer described in the instrumentation section. The thermal resistance of the gypsum board was taken as the value reported by ASHRAE (1985). The resistance of the multilayer walls was normalized with the extrapolated initial resistance to remove any dependency on the value used for the gypsum board. Thermal resistance value for the first three days were omitted from the analysis to eliminate the effect of transient heat conduction at the start of the conditioning period.

The daily average relative thermal resistance for each wall specimen is plotted as a function of elapsed time in Figure 12.

Glass Fiber Wall Specimen. In Figure 12a, the thermal resistance of the glass fiber wall specimen is seen to decrease slightly and linearly with elapsed time. A least-squares fit of the measured results indicates that the accumulation of moisture in the wall specimen decreased its thermal resistance by only 1.6%. From Figure 11a, very little moisture accumulated in the glass fiber insulation. Most of the decrease in wall thermal resistance is, therefore, attributed to the accumulation of bound moisture in the wood.

Cellulose Wall Specimen. A similar thermal resistance plot for the cellulose wall

specimen is given in Figure 12b. A decrease in thermal resistance of about 6% is seen to occur at day 16, followed by a gradual rise. The authors are unable to explain this variation in thermal resistance. One hypothesis is that it may result from two opposite-direction moisture transfers in the cellulose insulation. One of these is inward diffusion of bound moisture driven by the moisture concentration gradient. The other is outward vapor diffusion driven by the vapor partial pressure and temperature gradients. A "heat pipe" effect may be present, with the insulation serving as the wick material. The mathematical model presented in the paper does not account for these separate transport phenomena, and therefore cannot be used to support or refute the hypothesis.

CONCLUSIONS

A distributed-capacity, finite-difference model was presented for predicting the combined transfer of heat and water vapor within a multilayer plane wall. The model is one-dimensional and uses a single potential (i.e., vapor pressure) for predicting the moisture transfer rate.

Two plane wall specimens – each consisting of gypsum board with interior latex paint, cavity insulation, and white pine with exterior oil paint – were exposed to a step decrease in temperature and humidity at their exterior surfaces. Moisture was permitted to accumulate within the walls during a 34-day period. The moisture content of the white pine was predicted using a finite-difference model and compared to measured values.

The cored wood samples taken at the end of the conditioning period revealed a substantial lateral distribution in moisture content. This finding was unexpected because of precautions taken to design an experiment with one-dimensional moisture transfer. The lateral distribution in moisture content was well correlated with small variations in the wood surface temperature. Since the mathematical model was one-dimensional, it was unable to account for these lateral variations in moisture content.

However, when these final lateral variations in wood moisture content were averaged over the wood surface, the model appeared to predict with good agreement moisture accumulation in the wood. Here the term "moisture accumulation" denotes the difference between the final and initial moisture content. At the inside surface of the glass fiber wall specimen, the measured moisture accumulation was 10.6% compared to a predicted value of 9.3%. At the inside surface of the cellulose wall specimen, the measured moisture accumulation was 7.8% compared to a predicted value of 7.2%. For both wall specimens, a larger difference between measured and predicted values was observed at the outside surface of the wood.

Moisture accumulation within the wall specimens was found to decrease the apparent thermal resistance by 1.6% in the glass fiber wall specimen. In the cellulose wall specimen, a decrease in thermal resistance by about 6% is seen to occur at day 16, followed by a gradual rise. The authors were unable to predict this irregular behavior using the model presented in the paper.

Enhancements recommended for the model include extending the model to two dimensions, modeling nonisothermal moisture transfer in the bound and porous spaces within porous materials as separate processes, and using independently measured moisture transport properties as a function of moisture content and perhaps temperature.

ACKNOWLEDGMENTS

The authors thank the Office of Buildings and Community Systems of the Department of Energy for funding this research study.

NOMENCLATURE

A_n	=	constants in sorption isotherm and diffusion coefficient correlations	
C	=	Btu/lb-°F	specific heat
h	=	Btu/h-ft^2-°F	surface heat transfer coefficient
k	=	Btu/h-ft-°F	thermal conductivity of porous material
ℓ	=	ft	thickness of layer
L_w	=	ft	thickness of plane wall
$\dot{n}$	=	lb/ft^2-h	moisture mass flux
p	=	$in Hg_v$	water vapor pressure
R	=	h-ft^2-inHg/grain	moisture transfer resistance
t	=	h	time
T	=	°F	temperature
x	=	ft	distance measured from the exposed surface of porous material
γ	=	lb_m/lb_d	moisture content, dry basis
μ	=	lb/h-ft-inHg	permeability
λ	=	Btu/lb	latent heat of vaporization of water
M	=	perm	permeance or moisture conductance (1 perm = 1 grain/h-ft^2-inHg)
ϕ	=	(dimensionless)	relative humidity
ρ	=	lb/ft^3	mass density of dry material
θ	=	lb_m/ft^3	moisture content

Subscripts Refers to:

c	=	conditioning chamber or cup
d	=	dry property
e	=	effective property
f	=	air film property
g	=	saturated state
i	=	initial or insulation
m	=	moist property
n	=	layer index
N	=	number of layers
p	=	paint layer
r	=	environmental room
s	=	substrate
t	=	total

TABLE 1

Saturated Salt-in-Water Solutions Used for Sorption Isotherm Measurements

Salt	Formula	Equilibrium RH[1], %
Lithium Chloride	LiCl	11.3 ± 0.3
Magnesium Chloride	$MgCl_2 \cdot 6H_2O$	32.8 ± 0.2
Potassium Carbonate	K_2CO_3	43.2 ± 0.3
Sodium Bromide	NaBr	57.6 ± 0.4
Ammonium Chloride	NH_4Cl	78.6 ± 0.4
Potassium Chloride	KCl	84.3 ± 0.3
Potassium Nitrate	KNO_3	93.6 ± 0.6
Potassium Sulfate	K_2SO_4	97.3 ± 0.5

[1] At 77°F (25°C) from Greenspan (1977)

TABLE 2

Sorption Isotherm Coefficients[2] for Equation 13

Material	a_1	a_2	a_3
Gypsum Board	0.247	9.07	0.935
Cellulose Insulation	0.054	-0.320	0.928
Glass-fiber Insulation	0.101	53.6	0.931
White Pine	0.194	2.10	0.769

[2] Note: Coefficients apply to temperature of 71 F°(21 °C).

TABLE 3

Moisture Transport Properties of Materials

Material	Permeability grains/h-ft-inHg	Cup method
White Pine	0.74	wet
Cellulose Insulation	3.4	dry
Glass-fiber Insulation	4.5	dry

Material	Permeance grains/h-ft^2-inHg	Cup method
Gypsum Board (0.5 in)	48.	dry
Latex Paint System	5.4	wet
Oil-Base Paint System	2.8	wet

TABLE 4

Heat Transfer Properties

Material	Nominal[6] Thermal Conductivity Btu-in/hr-ft^2-°F	Density lb/ft^3	Specific Heat Btu/lb-°F
Gypsum Board	1.1[1]	41.8[3]	0.26[1]
White Pine	0.67[4]	22.8[3]	0.39[1]
Cellulose Insulation	0.30[2]	4.96[3]	0.33[1]
Glass-fiber Insulation	0.30[5]	0.716[3]	0.17[1]

[1] ASHRAE (1985)

[2] Tye (1974)

$$k = 0.2485 + 0.00980\rho + 0.005004(T - 75.2)$$

[3] measured

[4] Wilkes (1981)

$$k_r = 0.1791 + \rho(0.01874 + .05753\gamma)/(1 + \gamma)$$

$$k = k_r[1 + (0.001626 - 3.326X10^{-6}\rho)(T - 75)]$$

[5] Hust (1985)

$$k = -1.059X10^{-4} + 1.378X10^{-4}\rho + 7.714X10^{-5}T + 8.472X10^{-9}T^3/\rho + 1.339X10^{-3}\exp[-((T - 180)/75)^2]$$

[6] Values expressed at a mean temperature of 75 F° (24 °C) and a wood moisture content of 7.7%.

Note: Footnotes 2 and 4 in English units; footnote 5 in SI units.

REFERENCES

Anderson, L.O. 1972. "Condensation problems: their prevention and solution." USDA Forest Service Research Paper FPL 132. Madison, WI. Forest Products Laboratory: Madison, Wisconsin.

Andersson, A.C. 1985. "Verification of calculation methods for moisture transport in porous building materials." Document D6:1985 (ISBN 91-540-4325-5). Swedish Council for Building Research, Stockholm, Sweden.

ASHRAE. 1985. ASHRAE handbook – 1985 fundamentals, ch. 23. Atlanta: American Society of Heating, Refrigerating, and Air-Conditioning Engineers, Inc.

ASTM. 1988. "Standard test methods for water vapor transmission of materials." Annual Book of ASTM Standards, ASTM E96-80, pp. 855-864, Part 18.

Baxter, G.P., and Starkweather, H.W. 1916. "The efficiency of calcium chloride, sodium hydroxide, and potassium hydroxide as drying agents." Journal of the American Chemical Society, Vol. 38, No. 2, pp. 2038-2041.

Carnahan, B.; Luther, A.H.; and Wilkes, J.O. 1964. Applied numerical methods. NY: John Wiley & Sons, Inc.

Goff, J.A., and Gratch, S. 1946. "Low-pressure properties of water from -160 to 212°F." ASHVE Transactions, Vol. 52, pp. 95-122.

Greenspan, L. 1977. "Humidity fixed points of binary saturated aqueous solutions." Journal of Research, National Bureau of Standards, Vol. 81A, pp. 89-96.

Hust, J.G. 1985. "National Bureau of Standards certificate standard reference material 1451 thermal resistance – fibrous glass blanket." Gaithersburg, MD: National Bureau of Standards.

Incropera, F.P., and DeWitt, D.P. 1985 Fundamentals of heat and mass transfer, 2d edition. NY: John Wiley & Sons.

Kohonen, R. 1984. "A method to analyze the transient hygrothermal behavior of building materials and components." Publication 21 (ISBN 951-38-2020-3), Technical Research Centre of Finland, Espoo, Finland.

Simpson, W.T. 1971. "Equilibrium moisture content prediction for wood." Forest Products Journal, Vol. 21, No. 5, pp. 48-49.

Thomas, W.C., and Burch, D.M. 1989. "Experimental validation of a mathematical model for predicting water vapor sorption at interior building surfaces." ASHRAE Transactions, Vol. 95, Part 1.

Tye, R.P. 1974. "Heat transmission in cellulosic fiber insulation materials." Journal of Testing and Evaluation, Vol. 2, No. 3, pp. 176-179.

Wilkes, K.E. 1981. "Thermophysical properties data base activities at Owens-Corning Fiberglas." Proceedings of the ASHRAE/DOE - ORNL Conference Thermal Performance of the Exterior Envelope of Buildings, ASHRAE SP 28, pp. 662-677.

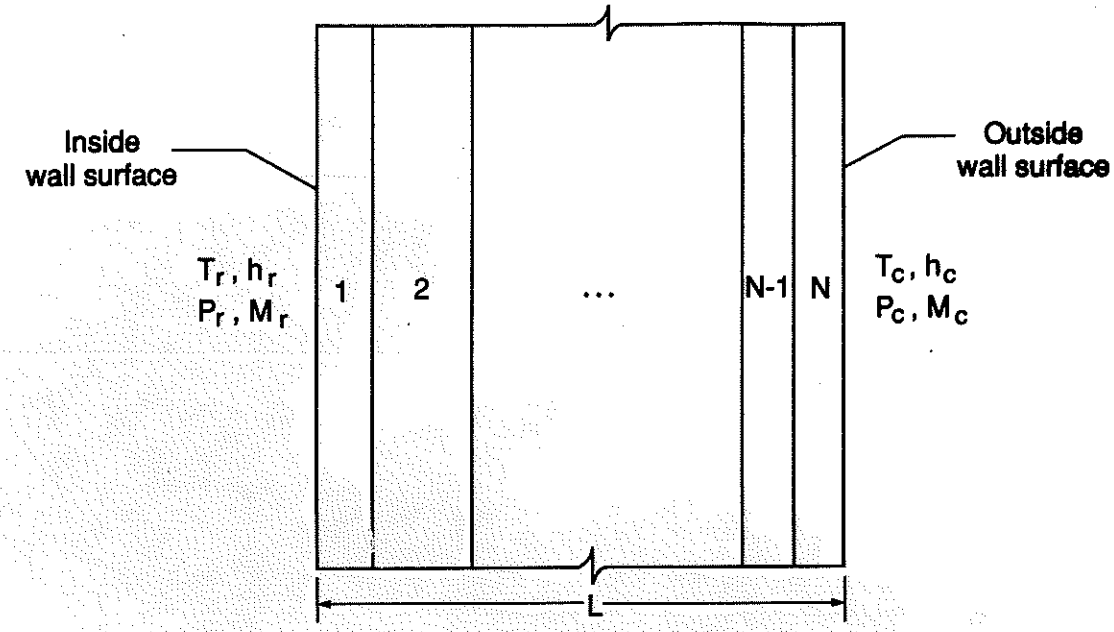

Figure 1. Schematic of slabs in series

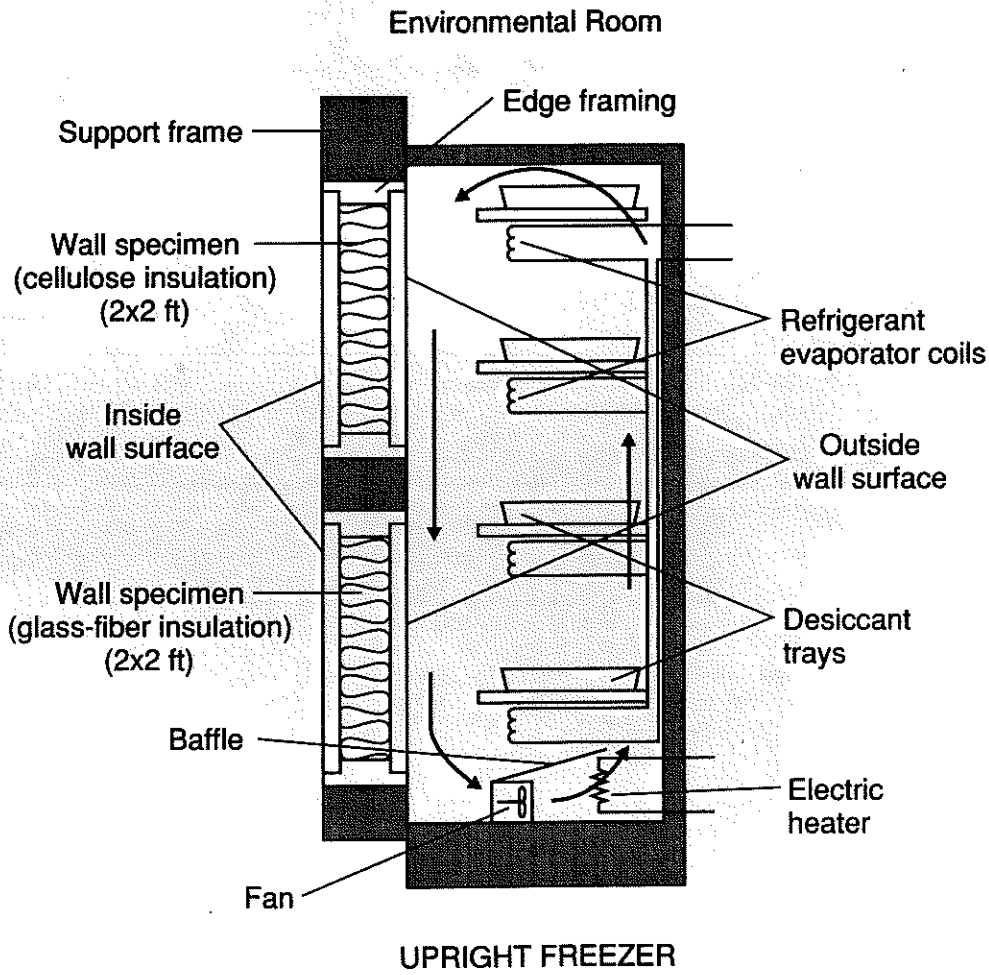

Figure 2. Schematic illustrating conditioning chamber

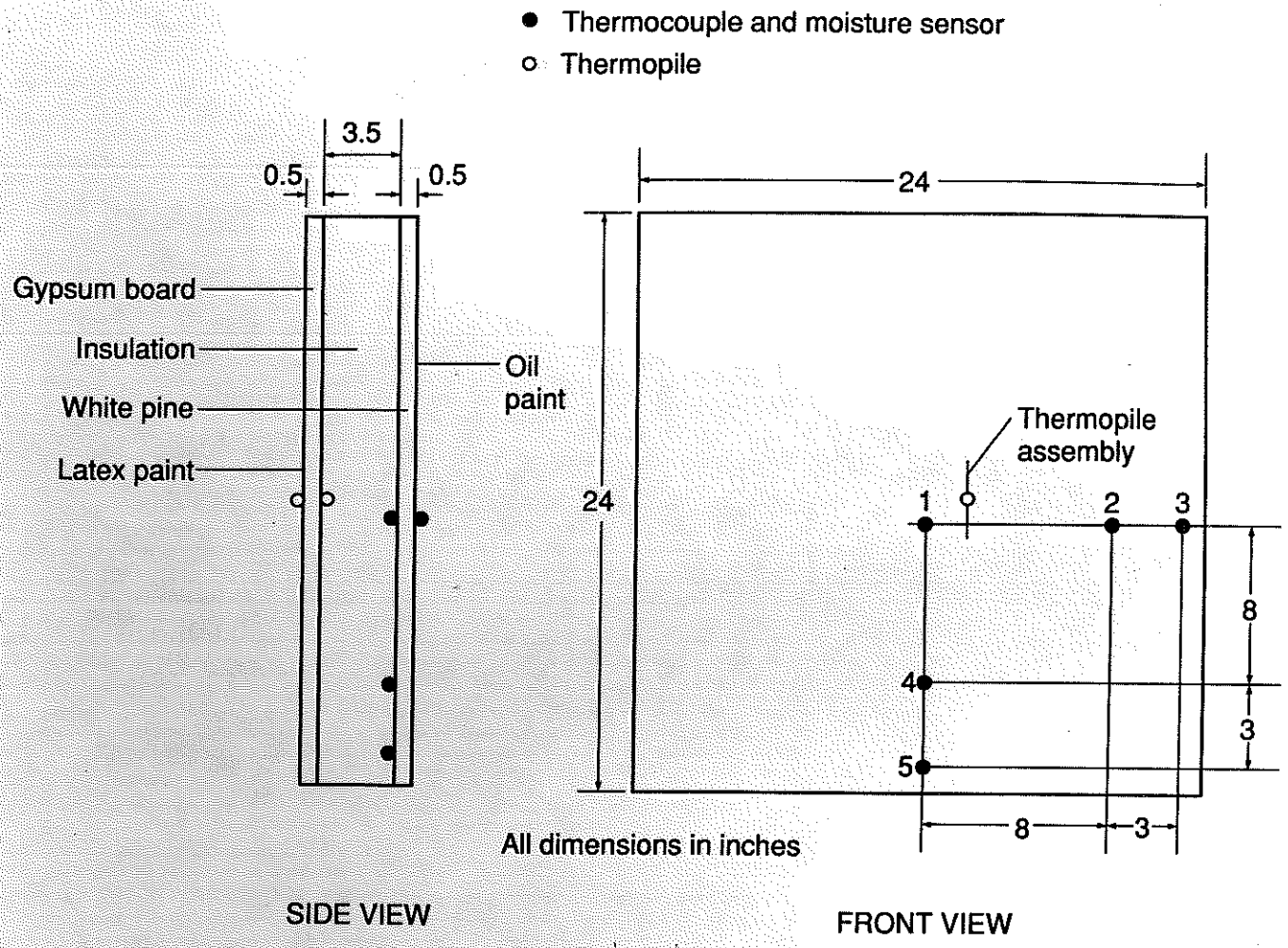

Figure 3. Schematic showing instrumentation

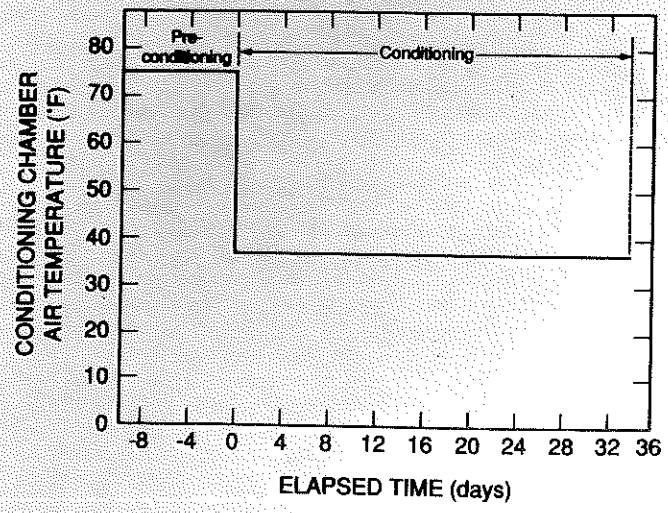

Figure 4a. Ambient conditions maintained in conditioning chamber—temperature

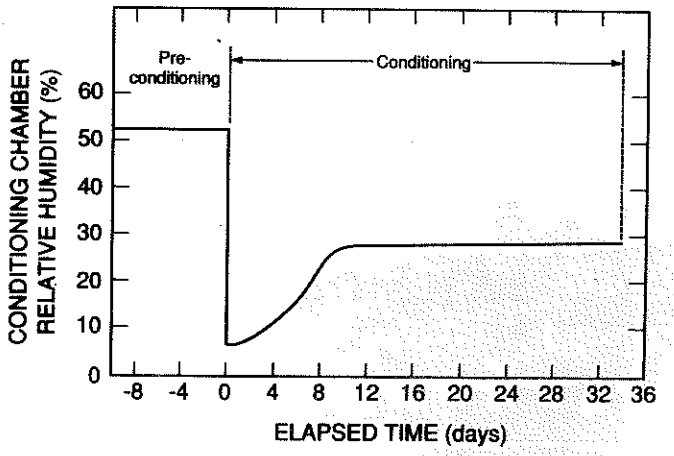

Figure 4b. Ambient conditions maintained in conditioning chamber—relative humidity

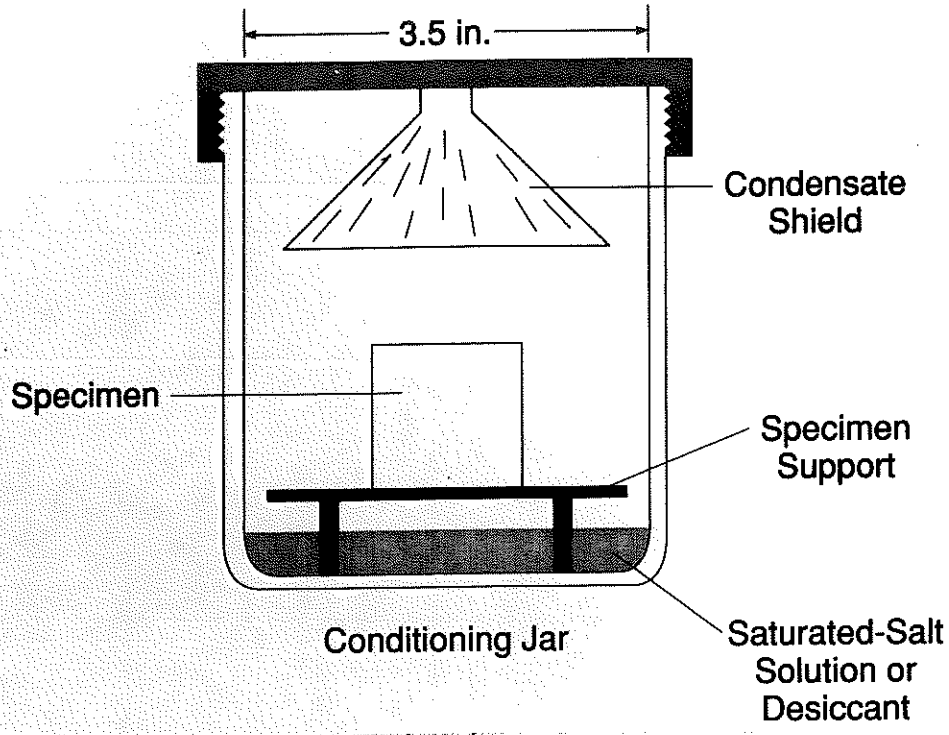

Figure 5. Schematic of conditioning jar

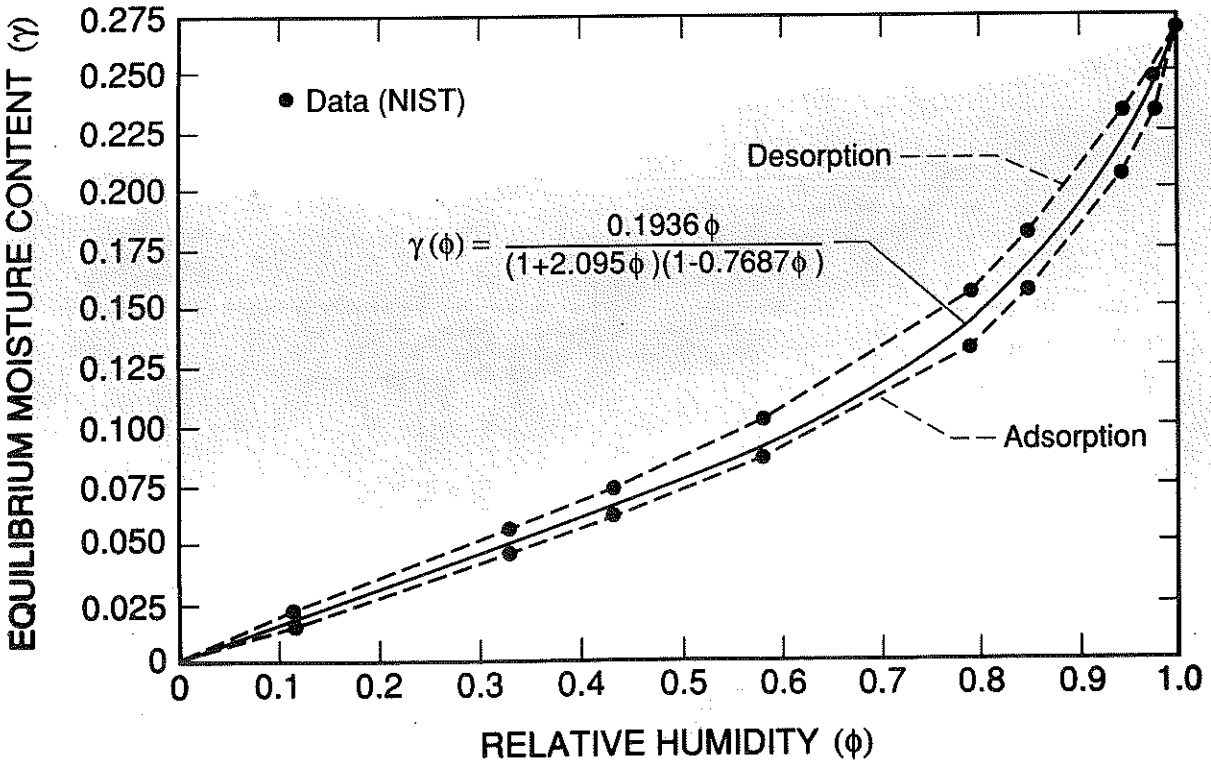

Figure 6. Sorption isotherm for white pine

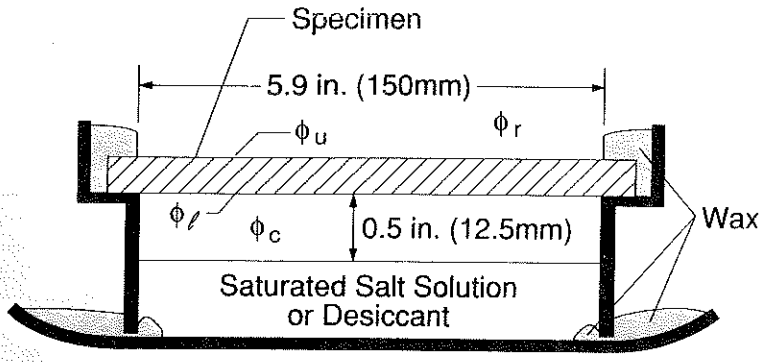

Figure 7. Schematic of permeance cup

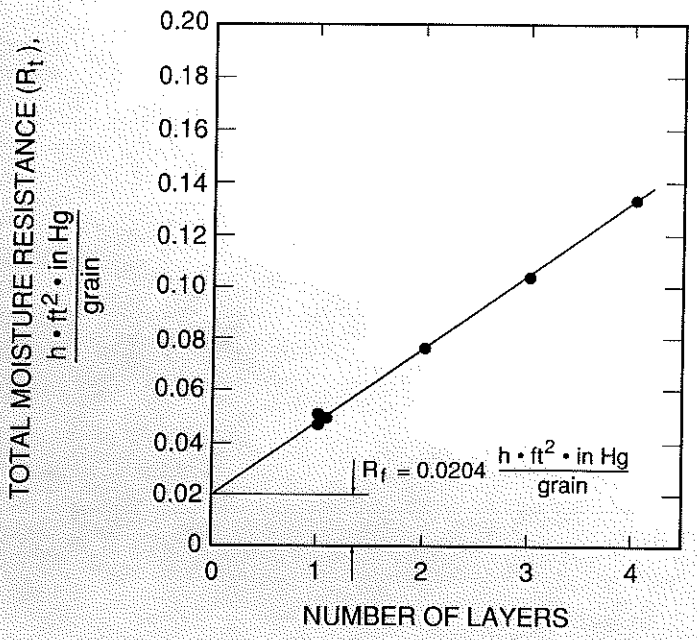

Figure 8. Total moisture resistance as a function of number of cork layers

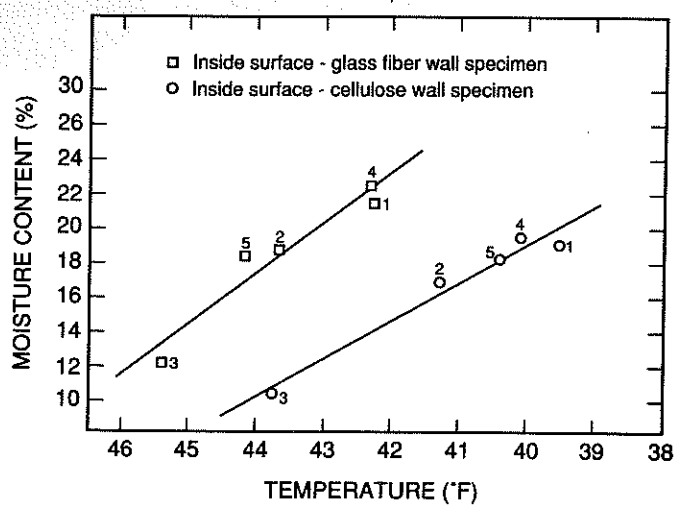

Figure 9. Moisture content vs. temperature for inside wood surface

Note: *The numbers above the symbols "o" and "□" denote the sensor locations given in Figure 3.*

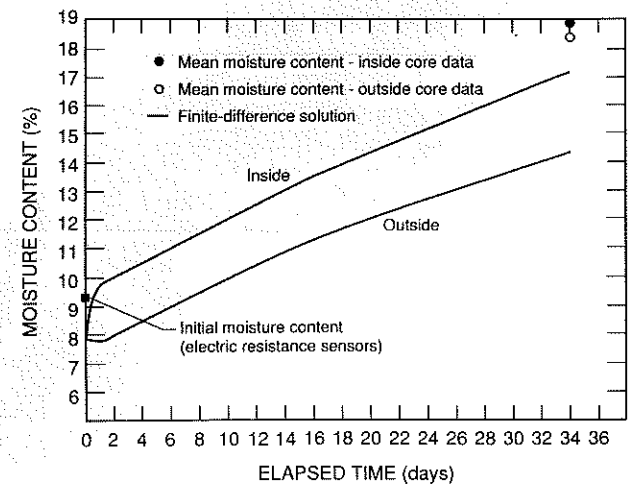

Figure 10a. *Wood moisture content vs. elapsed time—glass fiber wall specimen*

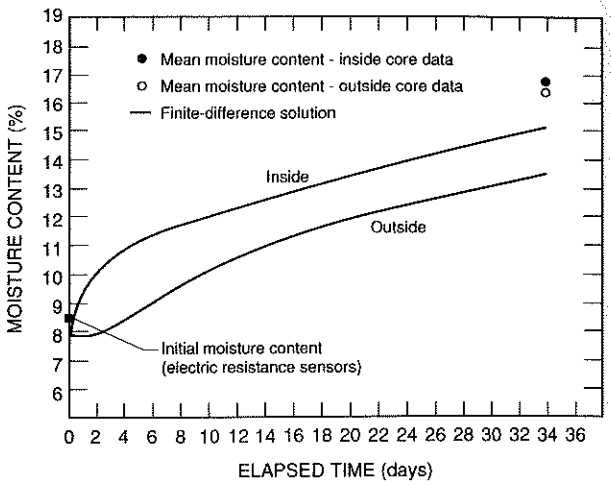

Figure 10b. *Wood moisture content vs. elapsed time—cellulose wall specimen*

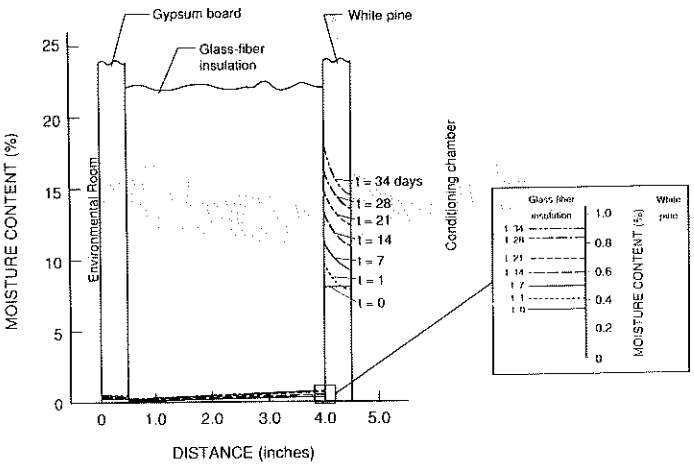

Figure 11a. *Predicted moisture content distribution for selected elapsed times—glass fiber wall specimen*

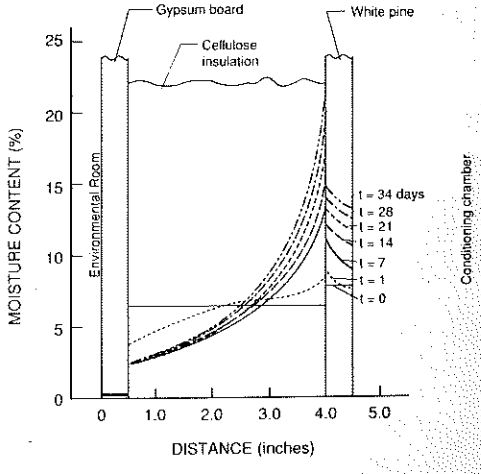

Figure 11b. *Predicted moisture content distribution for selected elapsed times—cellulose wall specimen*

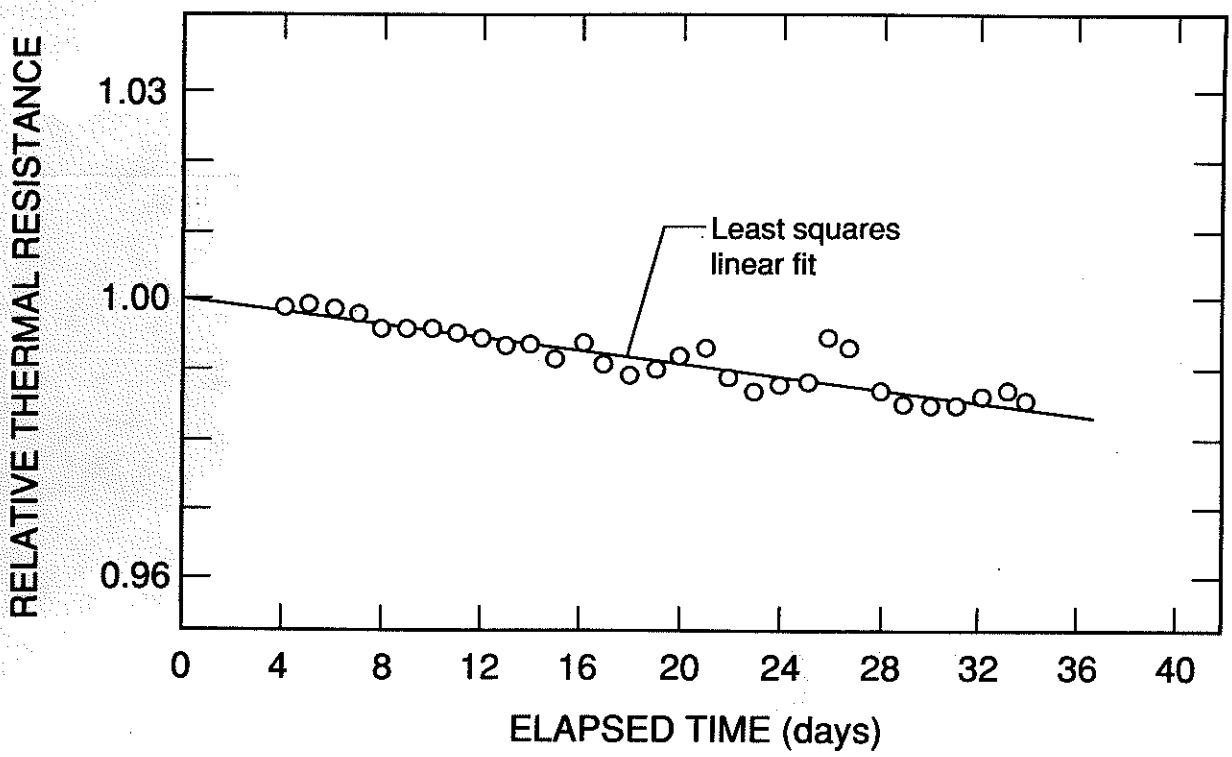

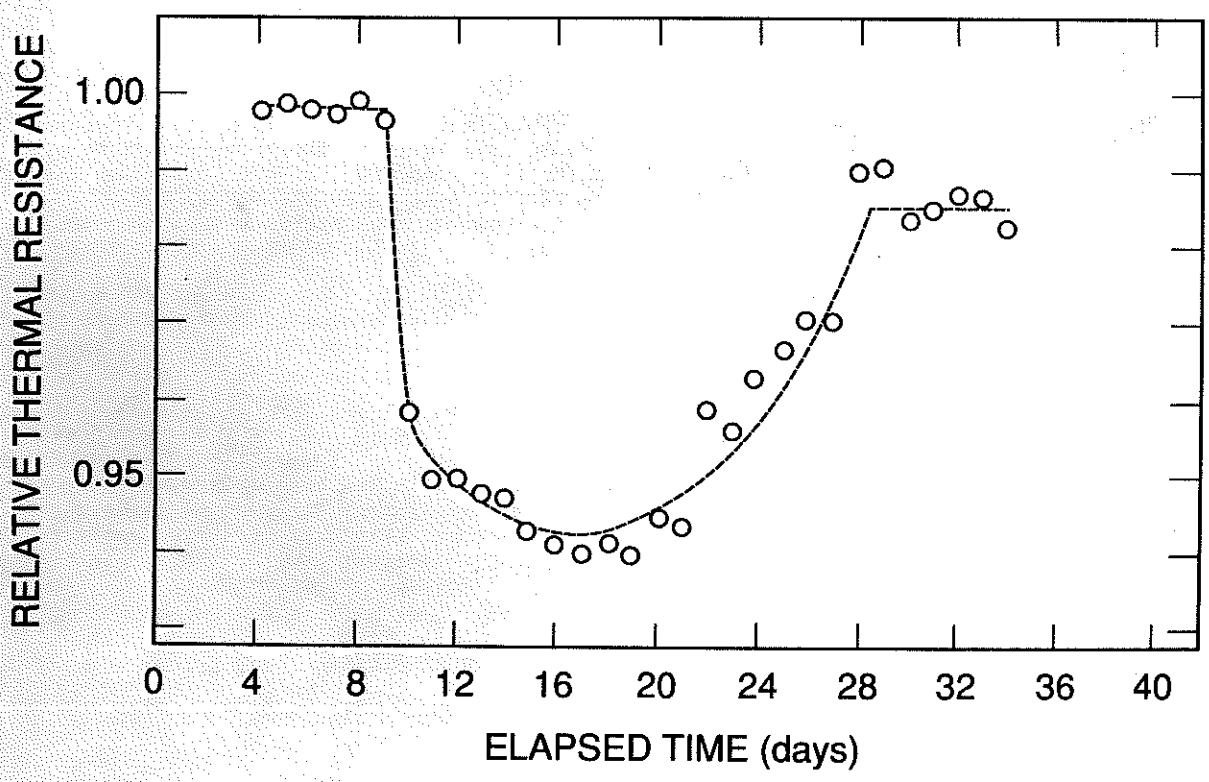

Figure 12. Wall thermal resistance vs. elapsed time